

Higher dimensional operators and LHC Higgs data : the role of modified kinematics

Shankha Banerjee¹, Satyanarayan Mukhopadhyay² and Biswarup Mukhopadhyaya³

^{1,3}*Regional Centre for Accelerator-based Particle Physics
Harish-Chandra Research Institute
Chhatnag Road, Jhusi, Allahabad - 211 019, India*

²*Kavli IPMU (WPI), The University of Tokyo,
Kashiwa, Chiba 277-8583, Japan.*

Abstract

The inclusion of higher-dimensional gauge invariant operators induces new Lorentz structures in Higgs couplings with electroweak gauge boson pairs. This in principle affects the kinematics of Higgs production and decay, thereby modifying the efficiencies of the experimental cuts compared to what simulations based on the standard model interactions yield. Taking some sample cases, we perform a rigorous analysis of how the efficiencies differ for various strengths of the additional operator vis-a-vis the standard model interactions, scanning over the values of both of them. While the response to cuts can be markedly different in some regions, we find that the sensitivity to new operator structures is relatively limited, so long as we remain confined to the 2σ regions around the best fit signal strengths measured at the Large Hadron Collider. We also show modifications to certain kinematical distributions including the new operators in the diphoton final state.

¹E-mail: shankha@hri.res.in

²E-mail: satya.mukho@ipmu.jp

³E-mail: biswarup@hri.res.in

1 Introduction

After the discovery of a new boson with a mass around 125 GeV at the Large Hadron Collider (LHC) [1, 2], there have been numerous studies attempting to pin down its properties, namely, its spin-parity and its couplings to standard model (SM) particles [3, 4, 5, 6, 7, 8]. The bosonic decay modes of this particle have been analyzed with greater precision than the fermionic modes by both the ATLAS and CMS collaborations, since the latter requires much more statistics and possibly the application of new search strategies. The signal-strengths reported in various channels by the experiments are broadly consistent with the SM predictions within about two standard deviations, and a preliminary analysis of spin-parity using the $ZZ^* \rightarrow 4\ell$ channel suggests that a CP-even scalar hypothesis is favoured over other alternatives [9]. Therefore, the accumulating evidence is in favour of an SM-like ($J^{PC} = 0^{++}$) Higgs boson, and we are going to assume so henceforth. Global fits of the Higgs data have been used by both experimentalists and theorists to derive bounds on possible deviations from the SM. Such deviations in the Higgs couplings can be parametrized either by including a multiplicative (or additive) constant to the SM coupling, or by including new Lorentz structures not present in the renormalizable SM Lagrangian. In the framework of the SM as an effective field theory valid below a cut-off scale Λ , higher-dimensional operators involving the SM fields and invariant under the SM gauge group can be used to capture possible new physics effects. A complete list of such operators has been written down in Ref. [10], while a minimal basis has been obtained rather recently in Ref. [11]. Such an approach is valid as long as there is no new light degree of freedom coupled to the SM sector below the scale Λ . Null results in LHC searches for new particles provide some motivation for this approach, although the presence of new particles charged under the SM gauge group is still viable even with masses around the electroweak symmetry breaking scale. Henceforth, we assume that there is no such new state, and work with the SM Lagrangian supplemented with dimension-6 operators involving SM gauge bosons and the SM Higgs doublet. As is well-known, although there exists one possible dimension-5 operator, it plays a role only in the generation of neutrino masses.

Electroweak precision measurements constrain the overall strength of the operators involving SM electroweak gauge bosons [12, 13]. However, such constraints come from one-loop contributions of these operators to the self-energy diagrams of the gauge-bosons, parametrized in terms of the so-called oblique corrections [14, 15]. In contrast, the Higgs boson couplings to W, Z or photon pairs can be affected at the tree level itself by a class of such operators, and therefore, it is possible to impose stronger constraints on their co-efficients using the already accumulated LHC Higgs data. This fact has been observed in several studies performing global fits to the Higgs data, and deriving limits on the operator co-efficients [16, 17, 18]. However, in most cases, these studies make an important assumption, namely, that the efficiencies of experimental cuts used for various final states are the same as the corresponding efficiencies in the SM case. To understand where the efficiency of experimental cuts enter the global fits, let us recall that the global fits are performed by comparing the experimentally observed signal strength ($\hat{\mu}_{X\bar{X}}$) in a channel $X\bar{X}$ with the corresponding signal strength predicted by a particular framework beyond the standard model

(BSM), $\mu_{X\bar{X}}$, which is defined as

$$\mu_{X\bar{X}} = \frac{[\sigma(pp \rightarrow H) \times \text{BR}(H \rightarrow X\bar{X}) \times \epsilon_{X\bar{X}}]_{\text{BSM}}}{[\sigma(pp \rightarrow H) \times \text{BR}(H \rightarrow X\bar{X}) \times \epsilon_{X\bar{X}}]_{\text{SM}}}, \quad (1)$$

where, $\epsilon_{X\bar{X}}$ denotes the efficiency of the experimental cuts applied to select a particular final state. Although the assumption that $(\epsilon_{X\bar{X}})_{\text{BSM}} = (\epsilon_{X\bar{X}})_{\text{SM}}$ can be justified if the Higgs couplings only receive a multiplicative modification to the SM one, it is not *a priori* clear whether such an assumption holds after the inclusion of dimension-6 operators. This is because these operators bring in new Lorentz structures to the Higgs-gauge boson couplings, which in turn modify the distributions of kinematic variables on which these cuts are imposed. Some of these distributions have been used in earlier studies, with special emphasis on the spin-parity determination of the newly discovered particle [19, 20, 21]. In this paper, we assume $J^{PC} = 0^{++}$ for this particle, and investigate how additional interaction terms with gauge boson pairs, gauge invariant and of higher dimension, affect Higgs phenomenology. With this in view, we subject the contributions of the additional operators to the cuts used on specific final states. Thus we demonstrate through rigorous Monte Carlo simulations how much the efficiencies can get modified, and to what extent they alter the bounds on the operator co-efficients. We use LHC Higgs search studies in the WW^* and $\gamma\gamma$ channels as examples, implement the cuts used by the ATLAS collaboration in our toy detector simulation, and determine the modified efficiencies for two such dimension-6 operators¹. We also simultaneously allow the modification of the SM coupling to the weak gauge bosons by a multiplicative constant, keeping the custodial $SU(2)$ symmetry intact. It should be mentioned that generically more than one higher-dimensional operator can be present in the effective low-energy theory with different coupling strengths. In that sense, our study with one operator considered at a time is illustrative, and focuses on the important effect of new Lorentz structures in the cut efficiencies. Moreover, the method developed here is of general utility in studying all possible higher-dimensional operators.

This paper is organized as follows. In section 2, we describe the higher dimensional operators considered, the modified Higgs-gauge boson couplings that they lead to, and constraints on them from electroweak precision tests. In section 3, we describe the set-up of our Monte-Carlo simulation, including its validation against the ATLAS Higgs search studies in the WW^* channel. The modified decay widths, cross-sections and efficiencies are presented in section 4, including simple parametrizations of each of these. Section 5 is devoted to the re-evaluation of constraints on these operators using a fit to the Higgs data in bosonic channels, while in section 6 we study the modified efficiencies in the associated production of Higgs. In section 7 we show the modifications to certain kinematic observables in presence of the new operators. We summarize our findings in section 8.

¹For an analysis of the modified efficiencies in the ZZ^* channel, we refer the readers to Ref. [22].

2 Dimension-6 operators and electroweak precision constraints

To illustrate the modification of experimental cut-efficiencies on including new Lorentz structures in Higgs-gauge boson interactions (henceforth called HVV interactions) we take the following dimension-6 operators as examples:

$$\begin{aligned}\mathcal{O}_{WW} &= \Phi^\dagger \hat{W}_{\mu\nu} \hat{W}^{\mu\nu} \Phi \\ \mathcal{O}_{BB} &= \Phi^\dagger \hat{B}_{\mu\nu} \hat{B}^{\mu\nu} \Phi,\end{aligned}\tag{2}$$

where, the field strength tensors for the $SU(2)_L$ and $U(1)_Y$ gauge groups are

$$\begin{aligned}\hat{W}_{\mu\nu} &= i\frac{g}{2}\sigma^a (\partial_\mu W_\nu^a - \partial_\nu W_\mu^a - g\epsilon^{abc}W_\mu^b W_\nu^c) \\ \hat{B}_{\mu\nu} &= i\frac{g'}{2} (\partial_\mu B_\nu - \partial_\nu B_\mu).\end{aligned}\tag{3}$$

Here, Φ denotes the SM Higgs doublet, σ^a are the Pauli matrices, and g, g' are the $SU(2)_L, U(1)_Y$ gauge couplings respectively. As mentioned in the introduction, the SM HWW and HZZ couplings can also get modified by a multiplicative factor in a general setting, where, for example, the SM Higgs doublet is part of a larger scalar sector. We therefore include the possibility of having the HWW and HZZ couplings modified by the same factor β , assuming custodial invariance. Since generically, in presence of an arbitrary number of extra scalar singlets or doublets, $\beta \leq 1$ [23], we scan the range $0 < \beta \leq 1$ in our analysis. One of the goals of this study is to determine to what extent β can be different from its SM value of 1, while including new dimension-6 operators. Taking these two modifications into account, the Lagrangian in the Higgs sector becomes

$$\mathcal{L} = \mathcal{L}_{SM}(\beta) + \frac{f_{WW}}{\Lambda^2} \mathcal{O}_{WW} + \frac{f_{BB}}{\Lambda^2} \mathcal{O}_{BB},\tag{4}$$

where, the operators \mathcal{O}_{WW} and \mathcal{O}_{BB} are given by equation 2, and the β dependence of the SM part comes from the following terms

$$\mathcal{L}_{SM}(\beta) \supset \beta \left(\frac{2m_W^2}{v} HW_\mu^+ W^{\mu-} + \frac{m_Z^2}{v} HZ_\mu Z^\mu \right).\tag{5}$$

Here, v denotes the vacuum expectation value of the Higgs field, and H denotes the Higgs boson. The Higgs couplings in \mathcal{L}_{SM} to fermions and gluons are not modified.

Since the new Higgs couplings generated by \mathcal{O}_{WW} and \mathcal{O}_{BB} , in particular the new Lorentz structures, are crucial to our discussion, we note down the additional HVV interactions generated by the operators in equation 2 [12, 13]:

$$\mathcal{L}_{HVV} \supset g_{HWW} HW_{\mu\nu}^+ W_-^{\mu\nu} + g_{HZZ} HZ_{\mu\nu} Z^{\mu\nu} + g_{H\gamma\gamma} H A_{\mu\nu} A^{\mu\nu} + g_{HZ\gamma} H A_{\mu\nu} Z^{\mu\nu},\tag{6}$$

where, $V_{\mu\nu} = \partial_\mu V_\nu - \partial_\nu V_\mu$, for $V = \{\gamma, W^\pm, Z\}$, and,

$$\begin{aligned} g_{HWW} &= -\left(\frac{gm_W}{\Lambda^2}\right) f_{WW} \\ g_{HZZ} &= -\left(\frac{gm_W}{\Lambda^2}\right) \frac{s^4 f_{BB} + c^4 f_{WW}}{2c^2} \\ g_{H\gamma\gamma} &= -\left(\frac{gm_W}{\Lambda^2}\right) \frac{s^2(f_{BB} + f_{WW})}{2} \\ g_{HZ\gamma} &= \left(\frac{gm_W}{\Lambda^2}\right) \frac{s(s^2 f_{BB} - c^2 f_{WW})}{c}. \end{aligned} \quad (7)$$

We have used the shorthand $c = \cos \theta_W$ and $s = \sin \theta_W$, θ_W being the Weinberg angle. The interaction terms involving the derivatives of the gauge fields bring in momentum dependent vertices, which are responsible for the modified kinematics in Higgs boson production via weak-boson fusion and associated production with a W or a Z , as well as the decay of the Higgs particle to electroweak gauge boson final states. The kinematics is affected most when the new interactions appear in both the production and decay processes, an example of which we shall discuss in sections 3 and 4. We should remark here that in $g_{H\gamma\gamma}$, only the new tree-level terms generated due to \mathcal{O}_{WW} and \mathcal{O}_{BB} have been considered. There will be additional contributions coming from the W boson loop (apart from the SM contribution modified by the inclusion of β , which we take into account), since now the HWW coupling also involves momentum-dependent terms. However, on naive power-counting in the number of loops and derivatives, these contributions are sub-leading, and the new divergences arising from this loop diagram will be cancelled by the next higher-order terms in the derivative expansion². With the current level of precision in the data, such terms can be safely neglected. Finally, though we have noted the new contribution to the $HZ\gamma$ vertex for completeness, there is no data in this channel so far, and therefore, the effect of the modification to this channel is sub-dominant.

The operators \mathcal{O}_{WW} and \mathcal{O}_{BB} contribute to the so-called Peskin-Takeuchi STU parameters [14, 15], and are therefore constrained by electroweak precision data [12, 13]. Following Ref. [13], the bounds at 95% C.L., taking one operator at a time, are given by

$$\begin{aligned} -24 \text{ TeV}^{-2} &< \frac{f_{WW}}{\Lambda^2} < 14 \text{ TeV}^{-2} \\ -79 \text{ TeV}^{-2} &< \frac{f_{BB}}{\Lambda^2} < 47 \text{ TeV}^{-2}. \end{aligned} \quad (8)$$

These bounds can change once we include the factor β in equation 5. However, as we shall see, the Higgs data puts much stronger constraints on these two operators compared to the precision data, and therefore, we do not consider modifications to the precision constraints in this study.

We note in passing that since the inclusion of the higher-dimensional operators in equation 4 modifies the HWW and HZZ vertices from their corresponding SM values, this will spoil the unitarity of $V_L V_L \rightarrow V_L V_L$ ($V = W, Z$) scattering amplitudes at high energies. For the values of operator coefficients allowed by the current Higgs data, the violation of

²We thank Adam Falkowski for clarifying this point.

unitarity appears at energies of a few TeV, with the exact value depending upon the specific choice of operators [24]. Since the higher-dimensional operators themselves arise from integrating out heavy fields of mass $\mathcal{O}(\Lambda)$ (for weakly coupled ultra-violet completions), one expects in general that the presence of these new degrees of freedom in the UV completion will eventually restore the unitarity of the full theory at high energies.

3 Simulation framework and validation using

$H \rightarrow WW^* + \geq 2j$ data

As noted in the previous section, we expect in general significant modifications to the kinematics in processes where the new Lorentz structures appear both in the production and decay vertices. An example of such a process is the production of Higgs boson via VBF and its subsequent decay to WW^* . The ATLAS collaboration has presented a detailed analysis of such a scenario in the $WW^* \rightarrow \ell^+ \nu \ell^- \bar{\nu}$ channel ($\ell = \{e, \mu\}$) in Ref. [25] using the 8 TeV, 20 fb $^{-1}$ data. The response of SM-type interactions to all the individual cuts can be readily checked from this analysis, which thus provides a much needed calibration for the simulation with additional operators. Therefore, we use this channel to set-up and validate our Monte Carlo as well as our detector simulation code.

We have used `FeynRules` [26] to extract the Feynman rules from the Lagrangian in equation 4, `MadGraph-5` [27] to generate the parton level events, `Pythia-6` [28] for parton shower and hadronization, and our own detector simulation code for analyzing the hadron-level events. Jet formation and underlying events have been simulated within the `Pythia` framework.

In the study of Higgs boson decaying to WW^* , followed by the semi-leptonic decay of the W 's, the ATLAS collaboration has considered three categories, namely, the production of Higgs in association with 0, 1, and ≥ 2 jets. In this part of the study, we consider only the ≥ 2 -jet category. According to Ref. [25], vector-boson fusion (VBF) and associated production with W or Z (called VH) are considered as signals in this category. For the WW^* final state, the VBF channel is picked out in the ATLAS analysis, by requiring a high invariant mass for the two leading jets in the forward region. The gluon-fusion production of Higgs is considered as a background. For a detailed description of the experimental cuts used, we refer the reader to Ref. [25]. To validate our Monte Carlo (MC) simulation, in tables 1 and 2, we compare the efficiencies of each of the experimental cuts obtained by our MC in the SM case, with the numbers reported by ATLAS, in the same and opposite flavour dilepton sub-categories respectively. As we can see from this comparison, our simulations agree with the ATLAS simulation to within 5% for all cuts except the one on m_{jj} , for which the difference is $\sim 15\%$. Our simulation shows a lower efficiency for this cut compared to ATLAS, and a possible reason for this is our inadequate modelling of detector effects for jets. Since the purpose of this part of the study is the overall validation of our MC, and in the subsequent sections we concentrate on the modification of efficiencies after including the dimension-6 operators within our own MC set-up, this difference is not expected to alter our main conclusions.

Cut	ATLAS efficiency	Our MC efficiency
$N_{b-jet} = 0$	0.68-0.76 (0.72)	0.74
$p_T^{tot} < 45$	0.81-0.93 (0.87)	0.88
$Z \rightarrow \tau\tau$ veto	0.86-1.00 (0.92)	0.95
$ \Delta y_{jj} > 2.8$	0.45-0.51 (0.48)	0.50
$m_{jj} > 500$	0.61-0.64 (0.62)	0.53
No jets in y gap	0.82-0.86 (0.84)	0.81
Both l in y gap	0.94-1.00 (0.97)	0.95
$m_{ll} < 60$	0.87-0.93 (0.90)	0.95
$ \Delta\phi_{ll} < 1.8$	0.89-0.96 (0.93)	0.92

Table 1: Comparison of the efficiencies of experimental cuts on the signal cross-section in the $H \rightarrow WW^* \rightarrow \ell^+ \nu \ell^- \bar{\nu}$ channel, for the $N_{jet} \geq 2$ category, demanding different flavour leptons ($e^+ \mu^- + \mu^+ e^-$) in the final state. The signal cross-section here refers to the sum of VBF and VH processes. The ATLAS numbers have been taken from Ref. [25], for which we show the 1σ range (the central value is written within brackets).

Cut	ATLAS efficiency	Our MC efficiency
$N_{b-jet} = 0$	0.69-0.77 (0.73)	0.73
$p_T^{tot} < 45$	0.84-0.95 (0.89)	0.87
$ \Delta y_{jj} > 2.8$	0.45-0.50 (0.48)	0.50
$m_{jj} > 500$	0.65-0.71 (0.68)	0.57
No jets in y gap	0.82-0.89 (0.85)	0.81
Both l in y gap	0.92-1.00 (0.96)	0.93
$m_{ll} < 60$	0.85-0.93 (0.89)	0.94
$ \Delta\phi_{ll} < 1.8$	0.88-0.97 (0.92)	0.90

Table 2: Same as table 1, for same-flavour leptons in the final state ($e^+ e^- + \mu^+ \mu^-$).

4 Modified efficiencies and signal strengths

After the validation of our MC simulation framework in the previous section, we are now in a position to determine the modified cut-efficiencies ($(\epsilon_{X\bar{X}})_{\text{BSM}}$ in equation 1) and signal strengths $\mu_{X\bar{X}}$ using the Lagrangian in equation 4. We first do so in the WW^* channel for

the ≥ 2 -jet category considered in section 3, by including only the operator \mathcal{O}_{WW} , where we expect the maximum modification. The efficiency then is a function of the parameters β and f_{WW} , and is given by

$$\epsilon_{WW^*+\geq 2\text{-jets}}(\beta, f_{WW}) = \frac{[\sigma(pp \rightarrow H)_{\text{VBF+VH}} \times \text{BR}(H \rightarrow WW^*)]_{\text{After Cuts}}}{[\sigma(pp \rightarrow H)_{\text{VBF+VH}} \times \text{BR}(H \rightarrow WW^*)]_{\text{Before Cuts}}}. \quad (9)$$

The theoretically calculated efficiencies are assumed here to be independent of radiative corrections. We evaluate the cross-sections before and after cuts by scanning over the parameters β and f_{WW} , and since they are found to be smooth functions of these parameters even after detector level simulations, we can parametrize them by simple polynomial functions of β and f_{WW} . The Higgs boson partial decay widths in the WW^* , ZZ^* , $\gamma\gamma$ and $Z\gamma$ channels are also functions of these two variables, while in the rest of the channels the partial widths are the same as in the SM. Since higher-order corrections are small in the aforementioned bosonic channels [29], we compute them at tree level, while for all other channels we have used the NNLO predictions from Ref. [30] for a Higgs mass of 125 GeV. The tree-level partial widths (in GeV) in these channels are rather accurately parametrized by the following expressions :

$$\begin{aligned} \Gamma_{H \rightarrow WW^*} &= 8.61 \times 10^{-4} \beta^2 + 8.51 \times 10^{-6} \beta f_{WW} + 2.95 \times 10^{-8} f_{WW}^2 \\ \Gamma_{H \rightarrow ZZ^*} &= 9.28 \times 10^{-5} \beta^2 + 4.77 \times 10^{-7} \beta f_{WW} + 1.00 \times 10^{-9} f_{WW}^2 \\ \Gamma_{H \rightarrow \gamma\gamma} &= 8.59 \times 10^{-7} - 8.04 \times 10^{-6} \beta - 4.36 \times 10^{-6} f_{WW} \\ &\quad + 1.77 \times 10^{-5} \beta^2 + 1.98 \times 10^{-5} \beta f_{WW} + 5.68 \times 10^{-6} f_{WW}^2 \\ \Gamma_{H \rightarrow Z\gamma} &= 3.75 \times 10^{-8} - 7.91 \times 10^{-7} \beta - 5.65 \times 10^{-7} f_{WW} \\ &\quad + 7.12 \times 10^{-6} \beta^2 + 1.06 \times 10^{-5} \beta f_{WW} + 3.82 \times 10^{-6} f_{WW}^2 \end{aligned} \quad (10)$$

For the above formulae and all subsequent ones involving f_{WW} , we have used a reference scale of $\Lambda = 1$ TeV, and for a different choice of the cut-off, the coefficients should be re-scaled according to the power of f_{WW} involved. Adding all the contributions, the total Higgs boson width becomes

$$\begin{aligned} \Gamma_{\text{tot}} &= [3.07 - 7.82 \times 10^{-3} \beta - 4.37 \times 10^{-3} f_{WW} \\ &\quad + 0.97 \beta^2 + 3.67 \times 10^{-2} \beta f_{WW} + 8.76 \times 10^{-3} f_{WW}^2] \times 10^{-3} \text{GeV}. \end{aligned} \quad (11)$$

Similarly, the tree-level total cross-section for the VBF and VH processes at 8 TeV LHC, before the application of selection cuts, can be expressed as follows

$$\sigma_{pp \rightarrow H+2\text{-jets}}(\text{VBF} + \text{VH}) = (2.0432 \beta^2 - 0.0330 \beta f_{WW} + 0.0030 f_{WW}^2) \text{ pb}. \quad (12)$$

By performing a scan over the (β, f_{WW}) parameter space, we compute the combined efficiency (defined in equation 9) of the basic trigger level cuts on jets and leptons as well as the subsequent ATLAS cuts listed in tables 1 and 2, and it is well-fit by the following function

$$\epsilon_{WW^*+\geq 2\text{-jets}} = \frac{50.98 \beta^4 + 121.76 \beta^3 f_{WW} + 22.85 \beta^2 f_{WW}^2 + 0.15 \beta f_{WW}^3 + 0.01 f_{WW}^4}{1601.43 \beta^4 + 3796.63 \beta^3 f_{WW} + 666.79 \beta^2 f_{WW}^2 - 1.98 \beta f_{WW}^3 + 0.73 f_{WW}^4}. \quad (13)$$

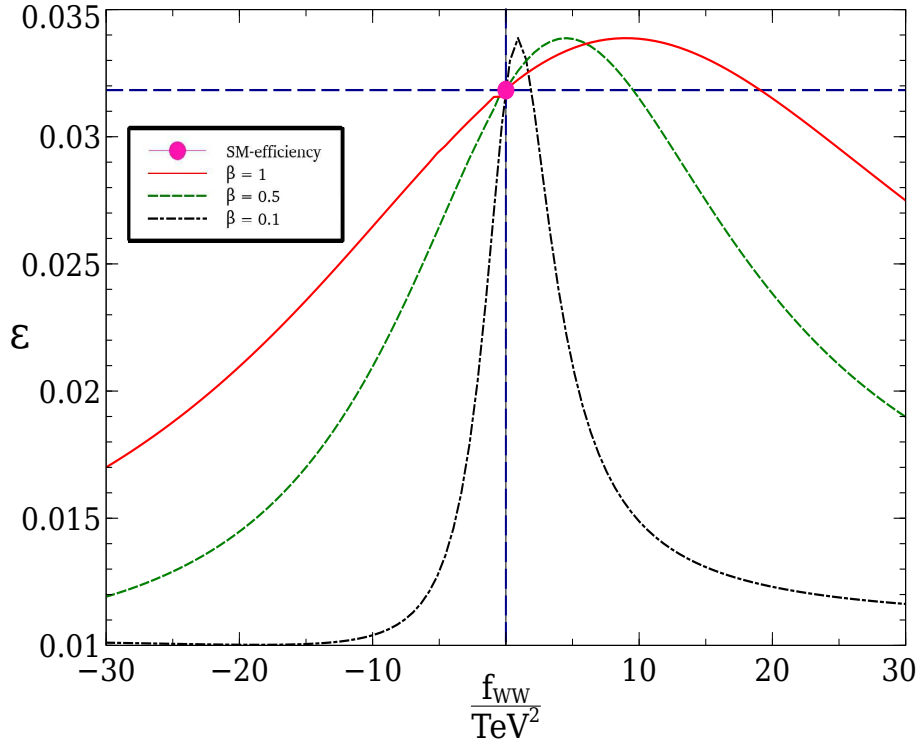


Figure 1: *The combined efficiency of all ATLAS cuts (ϵ) as a function of f_{WW} for different values of β , in the $H \rightarrow WW^* \rightarrow \ell^+ \nu \ell^- \bar{\nu}$ channel (≥ 2 -jets category) at 8 TeV LHC.*

In figure 1 we show the variation of $\epsilon_{WW^*+\geq 2\text{-jets}}$ as a function of f_{WW} for different values of β . The red (solid), green (dashed) and black (dot-dashed) curves correspond to $\beta = 1, 0.5$ and 0.1 respectively. For $f_{WW} = 0$, we recover the SM efficiency ($\epsilon_{\text{SM}} \simeq 0.032$) for all values of β . This fact confirms our expectation that only the introduction of new Lorentz structures changes the efficiencies, and a scaling of the SM coupling alone by the factor β does not. However, as we can see from this figure, although the overall features of the three curves are similar, for different values of β , the change in slopes are markedly different. Within the range of f_{WW} shown in this figure, for $\beta = 0.5$, the efficiency can reduce from its SM value by upto a factor of 2.5 or more, while for $\beta = 0.1$, it can drop by upto a factor of 3.

Combining equations 9 –13, we can now evaluate the signal strength μ for the $H \rightarrow WW^*$ mode in the ≥ 2 -jets category, for any value of β and f_{WW} . We emphasise that this calculation of the signal strength takes into account all the effects of the experimental cuts, and the resulting modification of their efficiencies compared to the SM case. This is one of our main results. In figure 2 we show the percentage difference of ϵ_{BSM} and ϵ_{SM} in this channel in the $\beta - f_{WW}$ plane. The ranges of the parameters have been restricted to a region consistent at 95% C.L., with the signal strength measured in this channel by ATLAS ($\hat{\mu} = 1.66 \pm 0.79$) [25]. For comparison, we also show the allowed region at 95% C.L. (grey

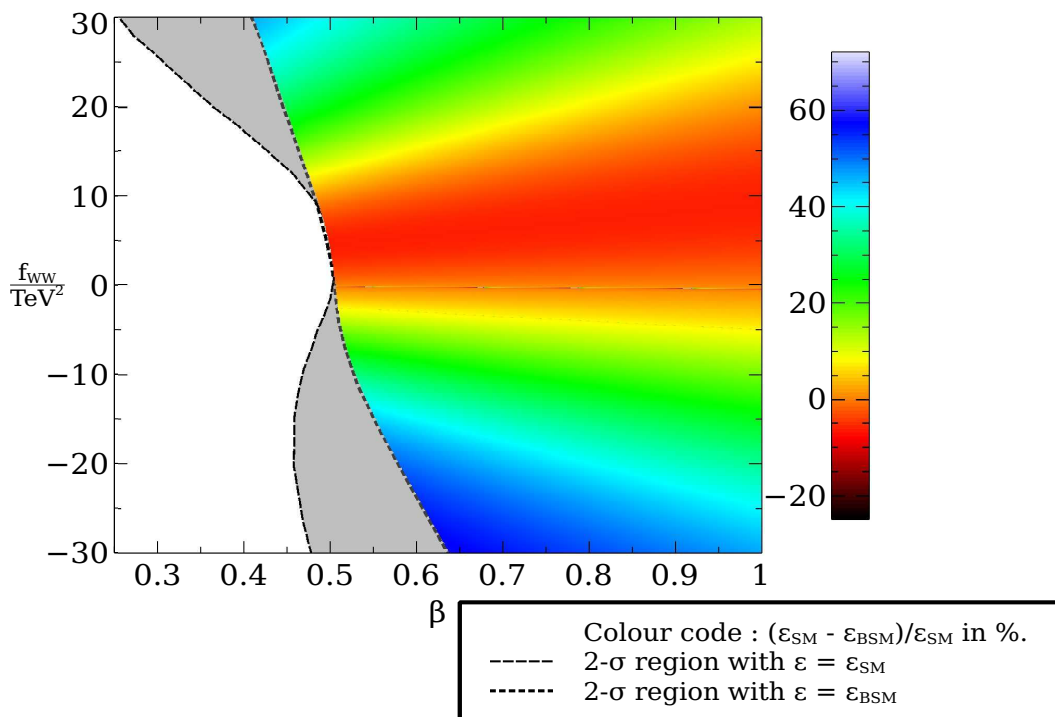


Figure 2: *Percentage modification of the combined efficiency of all cuts compared to the SM case, in the $H \rightarrow WW^* \rightarrow \ell^+ \nu \ell^- \bar{\nu}$ channel for the ≥ 2 -jets category at 8 TeV LHC. Only the region allowed at 95% C.L. after imposing the ATLAS signal-strength constraint in this channel is shown. For comparison, we also show the allowed region at 95% C.L. (grey shaded region to the right of the dashed curve), with the assumption $\epsilon_{\text{BSM}} = \epsilon_{\text{SM}}$.*

shaded region to the right of the dashed curve), with the assumption $\epsilon_{\text{BSM}} = \epsilon_{\text{SM}}$. It is clear that taking the efficiency modification into account significantly changes the parameter space allowed by the measurement in this channel. As we can also see from this figure, if this channel is considered on its own, the allowed region includes parameter points where the change in efficiency can be as large as 60%. Therefore, in a completely rigorous global analysis of the data, this modification should be taken into account.

5 Constraints using LHC Higgs data

In the previous section, we have seen that the operator \mathcal{O}_{WW} significantly modifies the final state kinematics in the $H + 2$ -jets channel (with $H \rightarrow WW^*$) and that a large region in the $\beta - f_{WW}$ parameter space is allowed by the current ATLAS measurement in this

particular final state. However, the signal strengths in other bosonic channels are modified by \mathcal{O}_{WW} as well. In this section, we therefore study the modifications to the inclusive $H \rightarrow WW^*$, $H \rightarrow ZZ^*$ and $H \rightarrow \gamma\gamma$ channels in presence of non-zero β and f_{WW} , and determine the most stringent possible constraints on these parameters. Before performing a global analysis with all the data taken together, we first analyze the constraints coming from each channel separately, in order to acquire a qualitative understanding. The signal strengths measured by the ATLAS and CMS collaborations, and a combination of the two experiments (assuming they are statistically independent) are shown in table 3. For the $H \rightarrow WW^* + 2\text{-jets}$ channel, only the ATLAS result is available at present.

Channel	ATLAS	CMS	Combined
$H \rightarrow \gamma\gamma$	$1.55^{+0.33}_{-0.28}$	$0.77^{+0.27}_{-0.27}$	$1.11^{+0.20}_{-0.20}$
$H \rightarrow WW^*$	$0.99^{+0.31}_{-0.28}$	$0.68^{+0.20}_{-0.20}$	$0.78^{+0.16}_{-0.16}$
$H \rightarrow ZZ^*$	$1.43^{+0.40}_{-0.35}$	$0.92^{+0.28}_{-0.28}$	$1.10^{+0.22}_{-0.22}$
$H \rightarrow WW^* + 2\text{-jets}$	$1.66^{+0.79}_{-0.79}$	NA	NA

Table 3: Signal strengths measured by the ATLAS and CMS collaborations, and a combination of the two experiments (assuming they are statistically independent) for the bosonic final states. For the $H \rightarrow WW^* + 2\text{-jets}$ channel, only the ATLAS result is available at present.

A measurement of the inclusive cross-section at 8 TeV LHC in the WW^* channel has also been reported by ATLAS, after unfolding all detector effects, and it is found to be (for $m_H = 125$ GeV) [25]

$$\sigma(pp \rightarrow H) \times \text{BR}(H \rightarrow WW^*) = 6.0 \pm 1.6 \text{ pb}, \quad (14)$$

which is slightly less than the expected SM cross-section (4.8 ± 0.7 pb), but consistent with it within the uncertainties. We find that this measurement of the inclusive cross-section puts a severe constraint in the $\beta - f_{WW}$ parameter space, and the 2σ allowed region after imposing this requirement is shown in figure 3. In the allowed region, to the right of the red (dashed) curve, f_{WW}/Λ^2 can be in the range $[-18 : 21] \text{ TeV}^{-2}$, while β is restricted to the range $[0.75 : 1.0]$. As we can see from equation 10, the relative magnitudes of the β^2 , βf_{WW} and f_{WW}^2 terms are similar for both $\Gamma_{H \rightarrow WW^*}$ and $\Gamma_{H \rightarrow ZZ^*}$. Therefore, their deviations from the SM will restrict β and f_{WW} in a similar range as well, especially since the signal strength measurements in both these channels have similar errors at the moment. Hence, we do not show the effect of the ZZ^* channel separately, although it is included in our global fit to the data in bosonic channels.

As seen in equation 7, \mathcal{O}_{WW} also affects the $H\gamma\gamma$ coupling, and therefore, the inclusive signal-strength measured in this channel. Since gluon fusion is the dominant production mechanism for this mode, and we do not find significant deviations in the kinematics if the momentum-dependent couplings appear only in the decay vertices, an appreciable change in the cut-efficiency factor is not expected for this channel, and we do not include a modified ϵ_{BSM} . In figure 3, along with the inclusive total cross-section constraint in

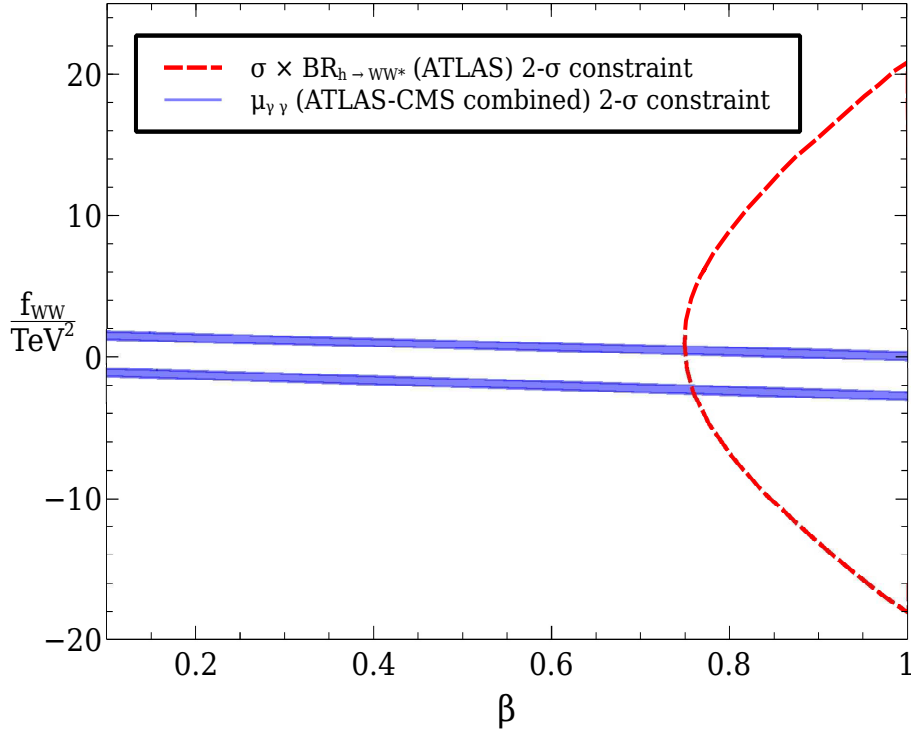


Figure 3: 2σ allowed regions in the $\beta - f_{WW}$ parameter space, after imposing the inclusive $\sigma(pp \rightarrow H) \times \text{BR}(H \rightarrow WW^*)$ cross-section measurement by ATLAS (to the right of the red dashed curve), and the combined ATLAS and CMS signal strength constraint in the $\gamma\gamma$ channel (blue-shaded bands).

the WW^* channel discussed above, we show the 2σ region, allowed by the combined signal strength measurement by ATLAS and CMS, $\hat{\mu}_{\gamma\gamma} = 1.11 \pm 0.2$. Only the two blue-shaded regions are allowed by the current data, restricting the values of f_{WW} to two narrow bands. For example, for $\beta = 1$ the allowed values of $f_{WW}/(1 \text{ TeV}^2)$ are in the two sub-regions $[-3.05, -2.46]$ and $[-0.25, 0.35]$. It is interesting to note that the intermediate region $-2.46 < f_{WW}/(1 \text{ TeV}^2) < -0.25$ is not allowed by the 2σ constraint. This is because, from equation 10, we can see that $\Gamma_{H \rightarrow \gamma\gamma}$ has a minimum at $f = -1.36$ for $\beta = 1$. Therefore, in this intermediate region around the minimum, the signal strength becomes lower than the 2σ allowed lowest value. Similarly, for $\beta = 0.1$, the allowed ranges for $f_{WW}/(1 \text{ TeV}^2)$ are $[-1.39, -0.85]$ and $[1.24, 1.80]$, and the minimum of $\Gamma_{H \rightarrow \gamma\gamma}$ is at $f = 0.21$. Since the operator \mathcal{O}_{BB} modifies the $H\gamma\gamma$ coupling in exactly the same form as \mathcal{O}_{WW} (see equation 7), these constraints on f_{WW} from the $\gamma\gamma$ data also apply to f_{BB} . The modified cut efficiencies in the VH channel in presence of \mathcal{O}_{BB} are studied in section 6.

As we can see from equation 10, for the $\gamma\gamma$ partial width, the contribution from \mathcal{O}_{WW} is comparable in magnitude to the loop-induced W-boson contribution, and therefore, values

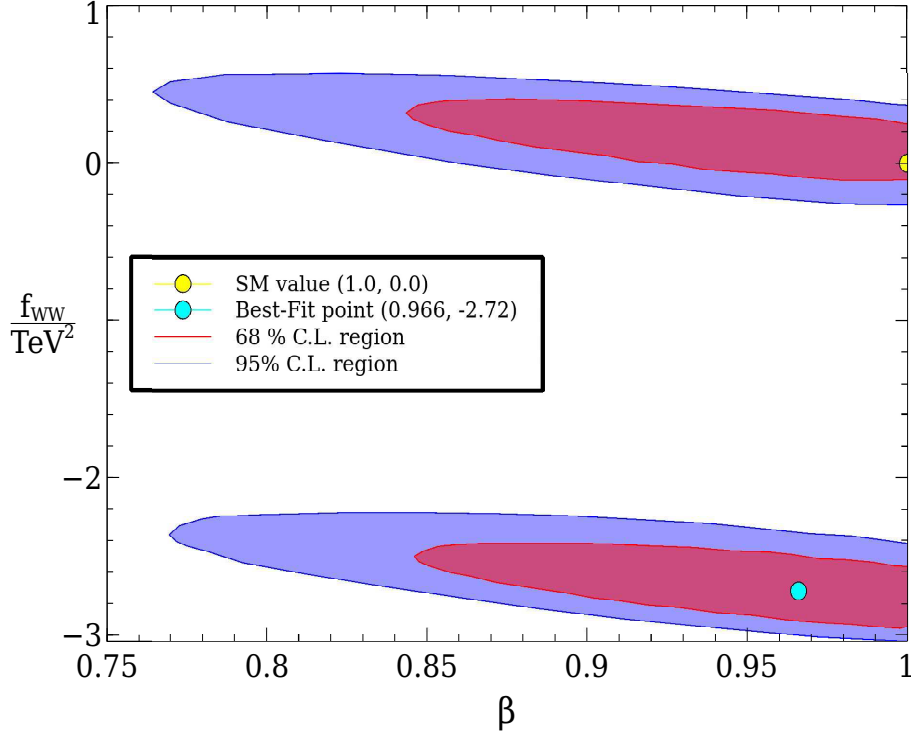


Figure 4: 68% and 95% C.L. allowed regions in the $\beta - f_{WW}$ parameter space, after performing a global fit using the data in all bosonic channels given in table 3. The best-fit and SM points are also shown.

of β as small as 0.1 with $|f_{WW}/(1 \text{ TeV}^2)| < 2$ are allowed by this constraint. This is not true for the WW^* inclusive cross-section constraint, where, the SM-like term contributes 2 orders of magnitude higher (see $\Gamma_{H \rightarrow WW^*}$ in equation 10), thereby restricting β to 0.75. Therefore, by comparing the $\gamma\gamma$ and WW^* inclusive constraints taken separately, we can learn that while large values of f_{WW} is disallowed by the former, small values of β are ruled out by the latter. A combination of all the constraints brings us to the global analysis using the data in the bosonic channels (see table 3), the result of which is presented in figure 4. The constraints on each of the parameters coming from the global fit is now easily understood in terms of the arguments given above. The best fit point corresponds to $\beta = 0.97$ and $f_{WW}/(1 \text{ TeV}^2) = -2.72$, which are very close to the SM point. However, there is still a small room for new physics effects described by \mathcal{O}_{WW} and β , as can be seen from the allowed regions at the 2σ level. We also show in figure 5 the $\Delta\chi^2$ distributions as a function of f_{WW} and β , after marginalizing over β and f_{WW} respectively. From this figure, we obtain the allowed range for β as

$$0.8 \leq \beta \leq 1.0 \quad 95\% \text{ C.L., marginalized over } f_{WW}. \quad (15)$$

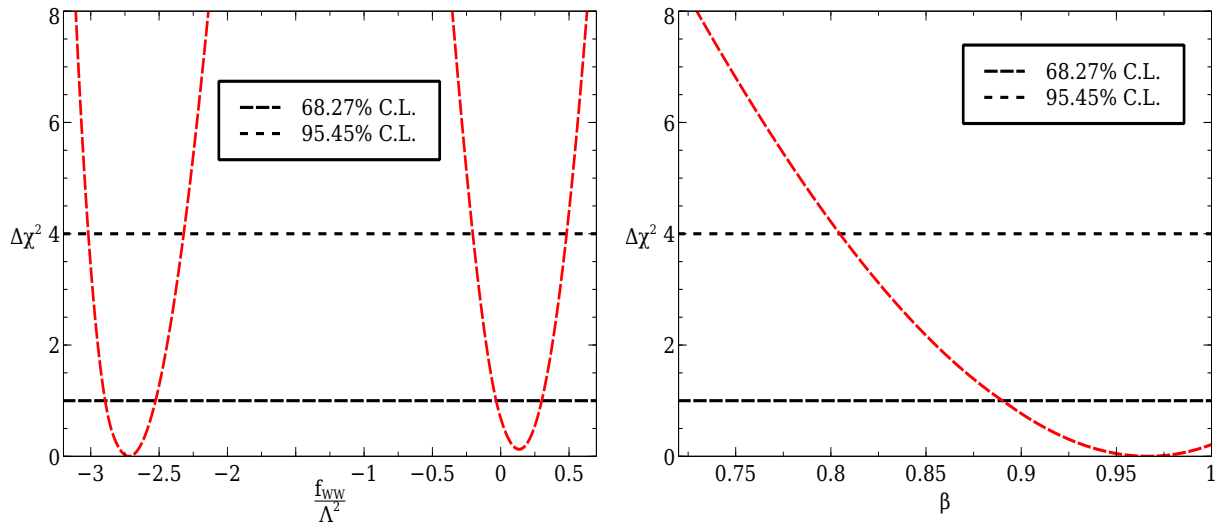


Figure 5: $\Delta\chi^2$ distributions as a function of f_{WW} (left) and β (right), after marginalizing over β and f_{WW} respectively. The allowed ranges at 68% and 95% C.L. are also shown by the horizontal dashed lines.

Similarly, the allowed range for f_{WW} is found to be

$$\frac{f_{WW}}{\text{TeV}^{-2}} \in [-3.02, -2.31] \cup [-0.20, 0.48] \quad 95\% \text{ C.L., marginalized over } \beta. \quad (16)$$

As far as the dimension-six operator \mathcal{O}_{WW} is concerned, this bound tells us that for a suppression scale $\Lambda = 1$ TeV, the co-efficient f_{WW} cannot be smaller than ~ -3 , or, in other words, if $f_{WW} = \mathcal{O}(1)$, $\Lambda \gtrsim 600$ GeV. This result is consistent with the present LHC direct search bounds on the mass of new coloured or uncoloured particles charged under the electroweak gauge group.

Two points are worth mentioning here. Firstly, it is true that the apparently allowed range of f_{WW} after fitting the data suggest rather modest change in cut efficiencies due to the presence of the additional operator. Still we consider the general demonstration of altered efficiencies over a range of the parameter space, quite substantially different in some cases, to be useful. Such altered efficiencies may plague our results, if, for example, overconstraining of f_{WW} has taken place because of event migration. Moreover, in our global fit, we could only include the modified cut efficiencies in the $WW^* + \geq 2$ -jets channel, and not in the other important bosonic channels like $\gamma\gamma$, ZZ^* and WW^* (inclusive), as the detailed information on the cut-flows for the latter channels are not yet presented by the experimental collaborations. Thus the 95% C.L. allowed regions obtained by a global fit with our current set-up is very similar to the region obtained using SM efficiencies. Once the detailed information of experimental cut-flows in all channels is available, our method can be extended to perform a fully rigorous global analysis. Secondly, even within the ‘apparently

allowed' range, it is worthwhile to look for modification in kinematic distributions due to the additional operators. For example, variables used in Boosted Decision Trees (BDT) can still bear the stamp of the higher-dimensional operators, as we shall see in section 7.

6 Associated production and higher dimensional operators

In section 4, we studied the change in efficiencies of the cuts used by ATLAS in the $H \rightarrow WW^*$ channel (≥ 2 -jet category), in presence of non-zero β and f_{WW} . These cuts were tailored to primarily select VBF events. In this section, we study the modification of cut-efficiencies in the associated production (VH) channel, in presence of \mathcal{O}_{WW} as well as \mathcal{O}_{BB} , taking their effects one at a time. As the operator \mathcal{O}_{BB} only modifies the HZZ and $H\gamma\gamma$ vertices, but not the HWW vertex (see equations 6, 7), its effect in the VBF channel is not significant³. We do not show the modification of efficiencies for the $H \rightarrow ZZ^*$ channel in the VH category, mainly because the cuts given in the corresponding experimental papers are not so transparently provided when compared to the WW^* and $\gamma\gamma$ final states.

Thus we focus here on the VH production of Higgs, where the Higgs decays to two photons and the vector boson (W or Z) decays hadronically. We closely follow the cuts used by ATLAS (see table 4) and study modifications to their efficiencies. The photon isolation criteria have been required to be $\Delta R_{\gamma\gamma} \geq 0.3$, $\Delta R_{\gamma j} \geq 0.4$ and $\Delta R_{\gamma l} \geq 0.4$, where j and l denote jets and leptons (e, μ), and $\Delta R_{ij} = \sqrt{(\eta_i - \eta_j)^2 + (\phi_i - \phi_j)^2}$, η and ϕ being the pseudorapidity and azimuthal angle respectively. In addition, a photon is considered isolated only if the total transverse energy around it in a cone of size $\Delta R = 0.4$ is less than 6 GeV. For further details on the cuts, we refer the reader to references [7, 31].

$100 \text{ GeV} < m_{\gamma\gamma} < 160 \text{ GeV}$
$60 \text{ GeV} < m_{jj} < 110 \text{ GeV}$
$ \Delta y_{jj} < 3.5$
$ \Delta \eta_{\gamma\gamma, jj} < 1$
$p_{T_t} > 70 \text{ GeV}$ ⁴

Table 4: *Cuts used for the VH channel with $H \rightarrow \gamma\gamma$ and $V \rightarrow jj$ in the low mass two-jet category (ATLAS). See references [7, 31] for details.*

³In the SM, the WW-fusion diagram contributes roughly 3 times to the VBF Higgs production cross-section, compared to the ZZ-fusion diagram, while the interference term is negligible ($\sim 1\%$) [29].

⁴ p_{T_t} is the diphoton transverse momentum orthogonal to the diphoton thrust axis in the transverse plane, as defined later in section 7.

As in equation 9, we define the efficiency for this channel as a function of β and f (f_{WW} or f_{BB}) as

$$\epsilon_{\gamma\gamma+2\text{-jets}(VH)}(\beta, f_{WW/BB}) = \frac{[\sigma(pp \rightarrow H)_{VH, V \rightarrow jj} \times \text{BR}(H \rightarrow \gamma\gamma)]_{\text{After Cuts}}}{[\sigma(pp \rightarrow H)_{VH, V \rightarrow jj} \times \text{BR}(H \rightarrow \gamma\gamma)]_{\text{Before Cuts}}}. \quad (17)$$

By performing a scan over the $(\beta, f_{WW/BB})$ parameter space, we obtain the combined efficiencies (for \mathcal{O}_{BB} and \mathcal{O}_{WW}) of the isolation cuts and the ATLAS cuts in table 4 and they are well fit by the following functions :

$$\begin{aligned} \epsilon_{\gamma\gamma+2\text{-jets}(VH)}(\beta, f_{BB}) = & \\ \frac{(3.75\beta^2 + 2.66\beta f_{BB} + 0.47f_{BB}^2) \times (0.15 - 1.34\beta + 0.01f_{BB} - 1.22\beta^2 - 0.05\beta f_{BB} - 1.3 \times 10^{-11}f_{BB}^2)}{(5.20\beta^2 + 3.68\beta f_{BB} + 0.65f_{BB}^2) \times (2.05 - 18.76\beta + 0.06f_{BB} - 17.57\beta^2 - 0.65\beta f_{BB} - 1.4 \times 10^{-10}f_{BB}^2)}, & \end{aligned} \quad (18)$$

$$\begin{aligned} \epsilon_{\gamma\gamma+2\text{-jets}(VH)}(\beta, f_{WW}) = & \\ \frac{(15.46\beta^2 - 1.33\beta f_{WW} + 0.05f_{WW}^2) \times (0.03 - 0.35\beta + 0.05f_{WW} - 8.88\beta^2 + 61.25\beta f_{WW} - 15.31f_{WW}^2)}{(0.64\beta^2 - 4.12\beta f_{WW} + 1.03f_{WW}^2) \times (-1.33 + 11.22\beta + 0.22f_{WW} - 4346.94\beta^2 + 392.44\beta f_{WW} - 14.86f_{WW}^2)}. & \end{aligned} \quad (19)$$

In equations 18 and 19, the denominator and the numerator represent $\sigma_{prod}^{VH} \times B.R.(H \rightarrow \gamma\gamma)$, before and after all the cuts respectively, and some common numerical factors between the two, like the total Higgs decay width have been cancelled out.

In figures 6 and 7, we show the variation of $\epsilon_{\gamma\gamma+2\text{-jets}(VH)}$ as a function of f_{BB} and f_{WW} respectively for different values of β . The red (solid), green (dashed) and black (dot-dashed) curves correspond to $\beta = 1, 0.5$ and 0.1 respectively. For $f_{BB} = 0$ or $f_{WW} = 0$ we recover the SM efficiency ($\epsilon_{SM} \sim 0.053$) in both the cases for all values of β . Within the range of f_{BB} shown in figure 6, the efficiency for $\beta = 0.5$ can change from its SM value by upto 8.7%, while for $\beta = 0.1$, it can increase by upto 19.7%. On the other hand, for the range of f_{WW} shown in figure 7, for $\beta = 0.5$ ($\beta = 0.1$), the efficiency can increase from its SM value by upto 14.7% (13.9%). Thus our overall conclusion is that the modification of cut efficiencies in the VH production mode is in general less pronounced than in the VBF Higgs production with $H \rightarrow WW^*$.

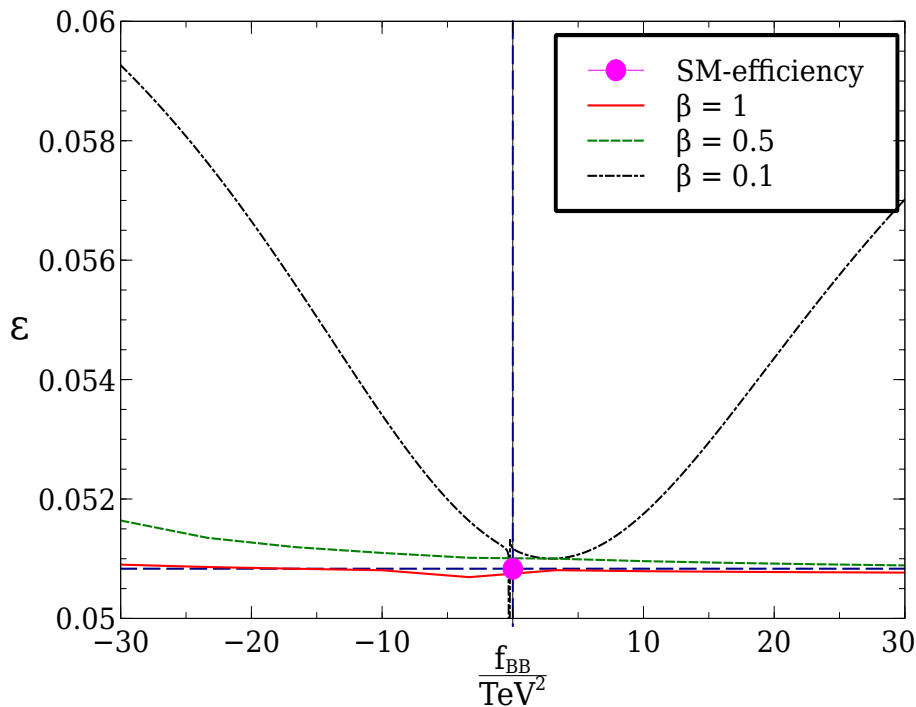


Figure 6: The combined efficiency of all ATLAS cuts (ϵ) as a function of f_{BB} for different values of β , in the $H \rightarrow \gamma\gamma$ channel (VH category) at 8 TeV LHC.

7 Modification to kinematic distributions : examples

Since the modifications of cut efficiencies discussed so far originate from changes in kinematic distributions, in this section, we explore some of these distributions in the presence of higher dimensional operators. Study of differential distributions is the next step in experimental analysis of the Higgs sector, and preliminary results with the current data have already been presented in Ref [32]. As an example we choose the diphoton channel in the VBF category [7, 31], and consider the operator \mathcal{O}_{WW} for illustration. All the distributions are shown after applying the standard trigger and isolation cuts for jets and photons. The kinematic variables considered are :

1. $\sqrt{\vec{p}_{Tj_1} \cdot \vec{p}_{Tj_2}}$, where j_1 and j_2 are the two tagged jets ordered in terms of their transverse momenta.

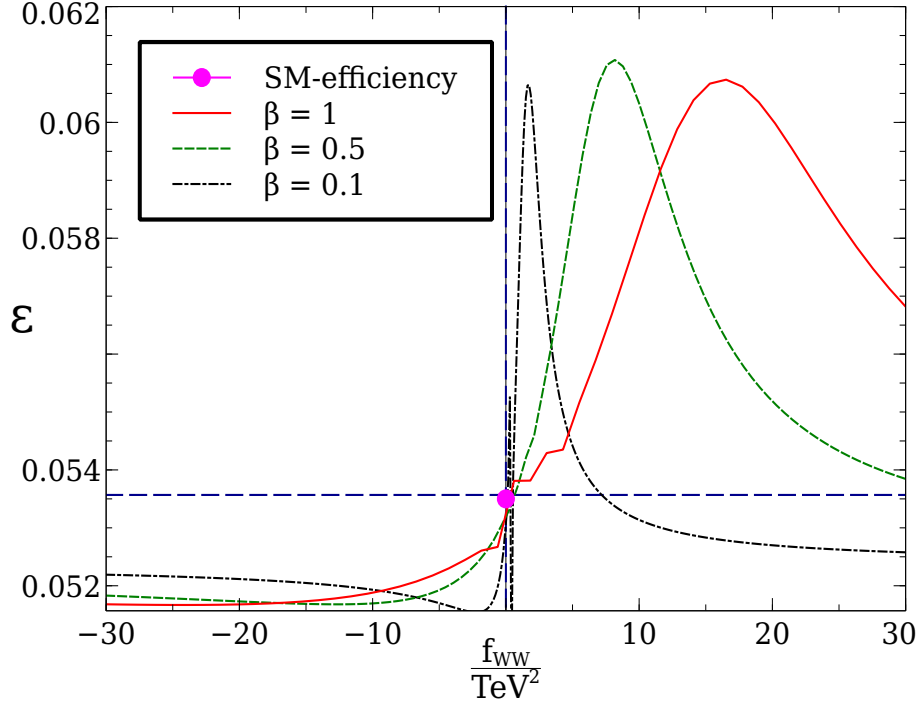


Figure 7: The combined efficiency of all ATLAS cuts (ϵ) as a function of f_{WW} for different values of β , in the $H \rightarrow \gamma\gamma$ channel (VH category) at 8 TeV LHC.

2. $|\Delta\eta_{j_1j_2}| = |\eta_{j_1} - \eta_{j_2}|$.
3. The invariant mass of the two tagged jets, $m_{j_1j_2}$. For this as well as the distributions listed below, the cut $|\Delta\eta_{j_1j_2}| > 2.8$ (see Ref. [33]) is imposed.
4. $p_{T_i} = |\vec{p}_T^{\gamma\gamma} \times \hat{t}|$, where $\hat{t} = \frac{\vec{p}_T^{\gamma 1} - \vec{p}_T^{\gamma 2}}{|\vec{p}_T^{\gamma 1} - \vec{p}_T^{\gamma 2}|}$ is the transverse thrust, $\vec{p}_T^{\gamma 1}$, $\vec{p}_T^{\gamma 2}$ are the transverse momenta of the two isolated photons and $\vec{p}_T^{\gamma\gamma} = \vec{p}_T^{\gamma 1} + \vec{p}_T^{\gamma 2}$ is the transverse momentum of the diphoton system [7, 31]. This and the subsequent distributions are subjected to the cuts $m_{j_1j_2} > 400$ GeV and $\Delta\phi_{\gamma\gamma,j_1j_2} > 2.6$, where $\Delta\phi_{\gamma\gamma,j_1j_2}$ is the azimuthal angle separation between the diphoton system and the system of the two tagged jets. The criterion of no hadronic activity in the rapidity gap between the two tagged jets is also imposed [33].
5. $\eta^* = \eta_{\gamma\gamma} - \frac{\eta_{j_1} + \eta_{j_2}}{2}$, where $\eta_{\gamma\gamma}$ is the pseudorapidity of the diphoton system.

6. $\Delta R_{\min}^{\gamma j}$ is the minimal ΔR between a photon and a tagged jet.

The last five kinematic variables form a subset of the inputs for the Boosted Decision Tree (BDT) employed by ATLAS for studying this channel [7, 31].

Figure 8 shows the normalised distributions in the above six variables for $\beta = 1$ and $f_{WW} = 0, \pm 10$ at the 8 TeV LHC. The values $f_{WW} = \pm 10$ are chosen for illustrative purpose only, since, as seen in section 5, although they are allowed by the LHC data in the WW^* channel, the current measurement in the $\gamma\gamma$ channel restricts f_{WW} to smaller values. Therefore, in figure 9 we show the aforementioned distributions in the SM, and for the parameters $\{\beta, f_{WW}\} = \{0.8, -3\}$ the latter being within the 2σ allowed range of the global fit (see figure 5). For both the above figures, the cut-off scale has been chosen as $\Lambda = 1$ TeV. We note that the distributions of $|\Delta\eta_{j_1 j_2}|$ have two peaks. The peak at $|\Delta\eta_{j_1 j_2}| = 0$ is due to VH contamination. Moreover, the relative heights of the two peaks change on introducing higher dimensional operators.

8 Summary

We have considered some illustrative dimension-6 operators for HVV interactions, and their potential contributions to the Higgs data, in conjunction with the SM-like operators. Parametrizing the strength of the additional interactions by f (f_{WW}/f_{BB}), and the simultaneous modification to the SM-like couplings to W and Z bosons by β , we show, after a detailed cut-based Monte Carlo analysis, how the efficiencies of different acceptance cuts are altered for various values of f and β . We find that in general there can be substantial modification of this kind, which underscores the importance of a detailed study of the effect of all such additional operators on the kinematics of various final states. When one further imposes the constraints on the (f, β) space as resulting from a global fit of the LHC data available till date, the f -parameters are in general restricted to rather modest values while β is restricted to be in the range $[0.8, 1]$. Thus the effects of cuts in the diboson channels may not be drastically different, unless there is ground for relaxing their constraints. In general, the VBF channel is more sensitive to the higher-dimensional operators than the

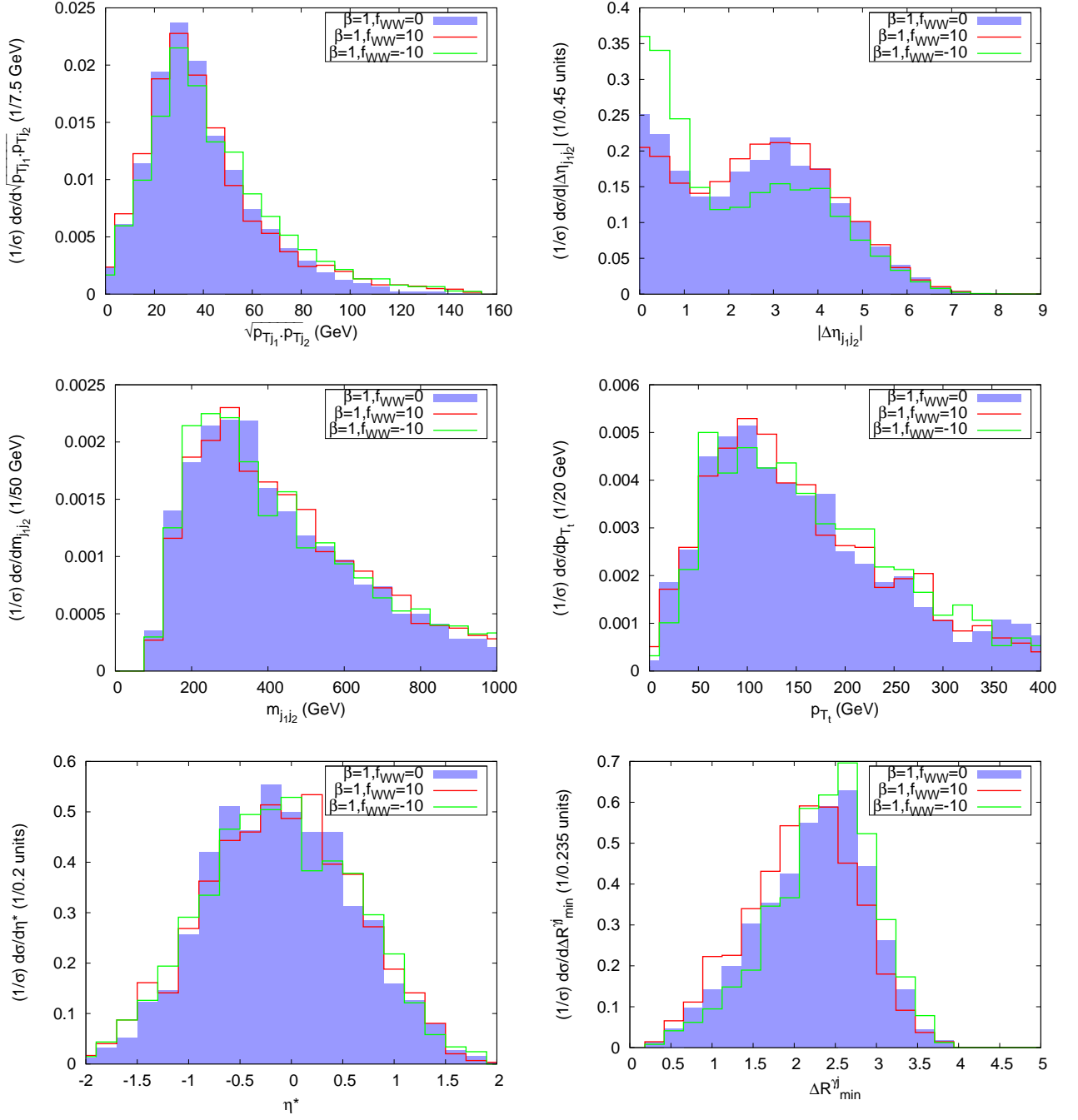


Figure 8: Normalised distributions in various kinematic variables for 8 TeV LHC, top row : $\sqrt{\vec{p}_{Tj_1} \cdot \vec{p}_{Tj_2}}$ (left) and $|\Delta\eta_{j_1j_2}|$ (right); middle row : $m_{j_1j_2}$ (left) and p_{T_i} (right); bottom row : η^* (left) and ΔR_{\min}^{jj} (right), for the parameter points $\{\beta = 1, f_{WW} = 0\}$ (shaded blue region), $\{\beta = 1, f_{WW} = 10\}$ (solid red line) and $\{\beta = 1, f_{WW} = -10\}$ (solid green line). The cut-off scale chosen is $\Lambda = 1$ TeV.

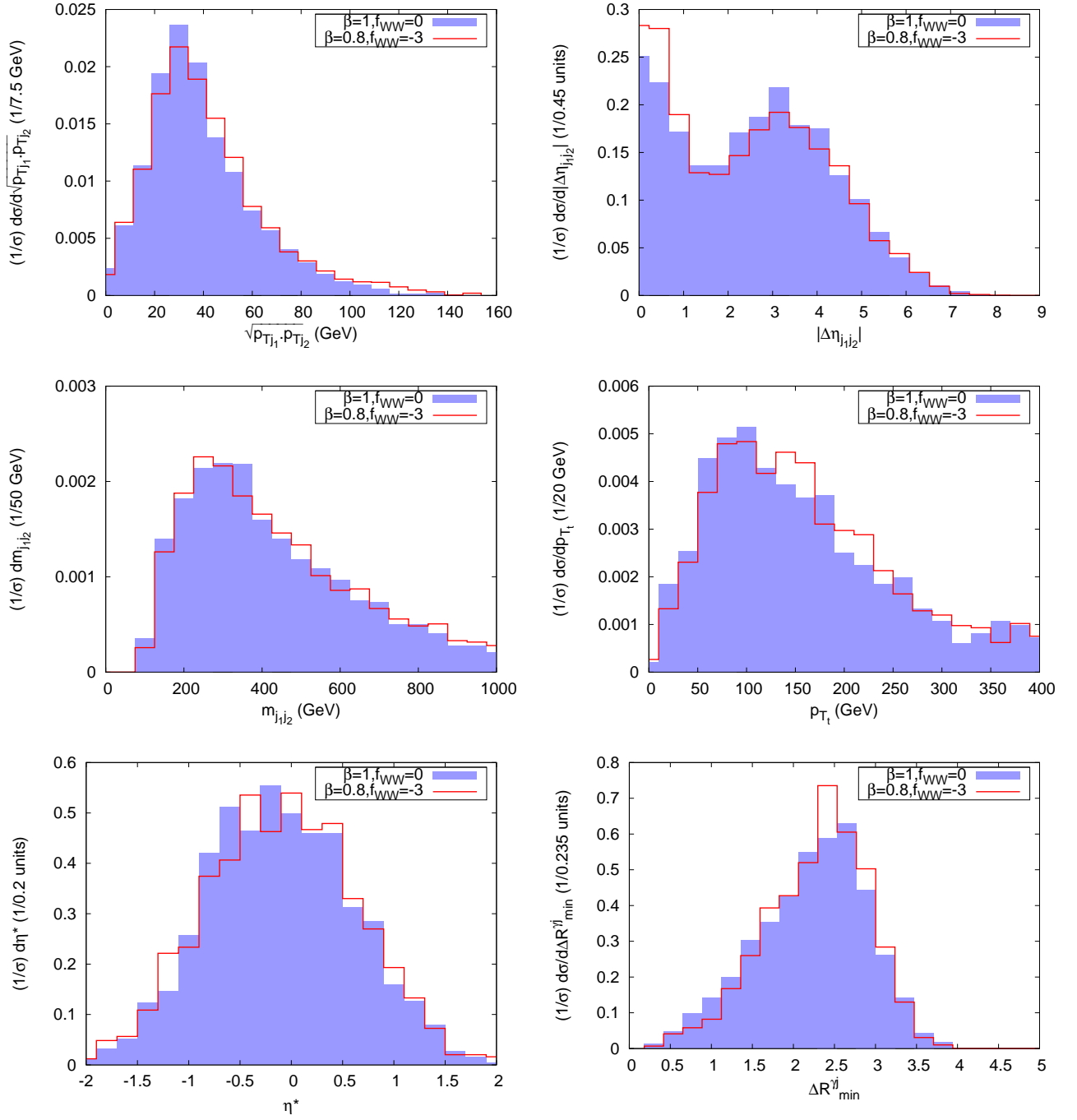


Figure 9: Normalised distributions in various kinematic variables for 8 TeV LHC, top row : $\sqrt{\vec{p}_{Tj_1} \cdot \vec{p}_{Tj_2}}$ (left) and $|\Delta\eta_{j_1j_2}|$ (right); middle row : $m_{j_1j_2}$ (left) and p_{Tl} (right); bottom row : η^* (left) and ΔR_{\min}^{η} (right), for the parameter points $\{\beta = 1, f_{WW} = 0\}$ (shaded blue region) and $\{\beta = 0.8, f_{WW} = -3\}$ (solid red line). The cut-off scale chosen is $\Lambda = 1$ TeV. Both the parameter points are allowed by the current data at 95% C.L.

gluon-fusion and VH production modes. We also present several kinematic distributions, some of which are used in BDT analyses, which can potentially bring out signatures of the new operators, even with moderate strength.

It should be remembered here that our analysis is purely phenomenological and data-driven; the assumption of any specific ultraviolet (UV) completion is deliberately avoided. In a specific UV completion scheme, more than one higher-dimensional operator relevant at the LHC scale may be generated, which can affect some of our conclusions. For example, with additional operators present, a situation as restrictive as indicated by figure 3 may not arise due to the accidental cancellation of different contributions. However, studying one operator at a time gives us valuable insight on how it typically affects various observables in the Higgs sector — an insight that is lost in the introduction of all operators of a given dimension simultaneously. In this spirit, we have explored two operators which can most significantly modify the interaction of the Higgs with a pair of electroweak gauge bosons.

Acknowledgment

We thank Atri Bhattacharya, Sanjoy Biswas, Ushoshi Maitra and Tanumoy Mandal for discussions and technical help. Useful comments from Bruce Mellado are also acknowledged. The work of SM is supported by World Premier International Research Center Initiative (WPI Initiative), MEXT, Japan. SB and BM acknowledge the funding available from the Department of Atomic Energy, Government of India, for the Regional Centre for Accelerator-based Particle Physics, Harish-Chandra Research Institute. Computational work for this study was partially carried out at the cluster computing facility at the Harish-Chandra Research Institute (<http://cluster.hri.res.in>).

References

- [1] G. Aad *et al.* [ATLAS Collaboration], Phys. Lett. B **716** (2012) 1.
- [2] S. Chatrchyan *et al.* [CMS Collaboration], Phys. Lett. B **716** (2012) 30.

- [3] For similar studies in this direction before the Higgs discovery, see,
 F. Bonnet, M. B. Gavela, T. Ota and W. Winter, Phys. Rev. D **85**, 035016 (2012);
 J. R. Espinosa, C. Grojean, M. Muhlleitner and M. Trott, JHEP **1205**, 097 (2012)
 P. P. Giardino, K. Kannike, M. Raidal and A. Strumia, JHEP **1206**, 117 (2012);
 T. Li, X. Wan, Y. -k. Wang and S. -h. Zhu, JHEP **1209**, 086 (2012); M. Rauch,
 arXiv:1203.6826 [hep-ph]; J. R. Espinosa, M. Muhlleitner, C. Grojean and M. Trott,
 JHEP **1209**, 126 (2012); J. Ellis and T. You, JHEP **1206** (2012) 140; D. Carmi,
 A. Falkowski, E. Kuflik and T. Volansky, JHEP **1207**, 136 (2012); M. Duhrssen,
 S. Heinemeyer, H. Logan, D. Rainwater, G. Weiglein and D. Zeppenfeld, Phys. Rev. D
70 (2004) 113009; R. Lafaye, T. Plehn, M. Rauch, D. Zerwas and M. Duhrssen, JHEP
0908 (2009) 009; M. Klute, R. Lafaye, T. Plehn, M. Rauch and D. Zerwas, Phys. Rev.
 Lett. **109**, 101801 (2012); A. Azatov, R. Contino, D. Del Re, J. Galloway, M. Grassi
 and S. Rahatlou, JHEP **1206**, 134 (2012).
- [4] I. Low, J. Lykken and G. Shaughnessy, Phys. Rev. D **86**, 093012 (2012); T. Corbett,
 O. J. P. Eboli, J. Gonzalez-Fraile and M. C. Gonzalez-Garcia, Phys. Rev. D **86**, 075013
 (2012); P. P. Giardino, K. Kannike, M. Raidal and A. Strumia, Phys. Lett. B **718**, 469
 (2012); J. Baglio, A. Djouadi and R. M. Godbole, Phys. Lett. B **716**, 203 (2012); J. Ellis
 and T. You, JHEP **1209**, 123 (2012); M. Montull and F. Riva, JHEP **1211**, 018 (2012);
 J. R. Espinosa, C. Grojean, M. Muhlleitner and M. Trott, JHEP **1212**, 045 (2012);
 D. Carmi, A. Falkowski, E. Kuflik, T. Volansky and J. Zupan, JHEP **1210** (2012)
 196; S. Banerjee, S. Mukhopadhyay and B. Mukhopadhyaya, JHEP **1210**, 062 (2012);
 F. Bonnet, T. Ota, M. Rauch and W. Winter, Phys. Rev. D **86**, 093014 (2012); T. Plehn
 and M. Rauch, Europhys. Lett. **100**, 11002 (2012); A. Djouadi, arXiv:1208.3436 [hep-
 ph]; B. Batell, S. Gori and L. -T. Wang, JHEP **1301** (2013) 139; G. Moreau, Phys. Rev.
 D **87**, 015027 (2013); G. Bhattacharyya, D. Das and P. B. Pal, Phys. Rev. D **87**, 011702
 (2013); D. Choudhury, R. Islam and A. Kundu, arXiv:1212.4652 [hep-ph]. G. Belanger,
 B. Dumont, U. Ellwanger, J. F. Gunion and S. Kraml, JHEP **1302**, 053 (2013).
- [5] M. Klute, R. Lafaye, T. Plehn, M. Rauch and D. Zerwas, Europhys. Lett. **101** (2013)
 51001; C. Grojean, E. E. Jenkins, A. V. Manohar and M. Trott, JHEP **1304**, 016

- (2013); K. Cheung, J. S. Lee and P. -Y. Tseng, JHEP **1305**, 134 (2013); J. Elias-Mir, J. R. Espinosa, E. Masso and A. Pomarol, JHEP **1308**, 033 (2013); J. Ellis, V. Sanz and T. You, arXiv:1303.0208 [hep-ph]; P. P. Giardino, K. Kannike, I. Masina, M. Raidal and A. Strumia, arXiv:1303.3570 [hep-ph]; R. Contino, M. Ghezzi, C. Grojean, M. Muhlleitner and M. Spira, JHEP **1307**, 035 (2013); J. Ellis and T. You, JHEP **1306**, 103 (2013); A. Djouadi and G. Moreau, arXiv:1303.6591 [hep-ph]; W. -F. Chang, W. -P. Pan and F. Xu, Phys. Rev. D **88**, 033004 (2013); T. Corbett, O. J. P. Eboli, J. Gonzalez-Fraile and M. C. Gonzalez-Garcia, arXiv:1304.1151 [hep-ph]; B. Dumont, S. Fichet and G. von Gersdorff, JHEP **1307**, 065 (2013); J. Elias-Miro, J. R. Espinosa, E. Masso and A. Pomarol, arXiv:1308.1879 [hep-ph]; M. B. Einhorn and J. Wudka, arXiv:1308.2255 [hep-ph]; A. Pomarol and F. Riva, arXiv:1308.2803 [hep-ph].
- [6] Talk given by Michael Duehrssen on behalf of the ATLAS collaboration, <https://indico.cern.ch/getFile.py/access?contribId=231&sessionId=15&resId=0&materialId=0>, G. Aad *et al.* [ATLAS Collaboration], arXiv:1307.1432 [hep-ex].
- [7] G. Aad *et al.* [ATLAS Collaboration], arXiv:1307.1427 [hep-ex].
- [8] Talk given by Josh Bendavid on behalf of the CMS collaboration, <https://indico.cern.ch/getFile.py/access?contribId=430&sessionId=15&resId=0&materialId=0>, CMS conference note, <http://cds.cern.ch/record/1542387?ln=en>
- [9] ATLAS conference note, <https://atlas.web.cern.ch/Atlas/GROUPS/PHYSICS/CONFNOTES/ATLAS-CONF-2013-013/>
- [10] W. Buchmuller and D. Wyler, Nucl. Phys. B **268**, 621 (1986).
- [11] B. Grzadkowski, M. Iskrzynski, M. Misiak and J. Rosiek, JHEP **1010**, 085 (2010).
- [12] K. Hagiwara, R. Szalapski and D. Zeppenfeld, Phys. Lett. B **318**, 155 (1993).
- [13] M. C. Gonzalez-Garcia, Int. J. Mod. Phys. A **14**, 3121 (1999).

- [14] M. E. Peskin and T. Takeuchi, Phys. Rev. Lett. **65**, 964 (1990); M. E. Peskin and T. Takeuchi, Phys. Rev. D **46**, 381 (1992).
- [15] G. Altarelli, R. Barbieri and F. Caravaglios, Nucl. Phys. B **405**, 3 (1993).
- [16] E. Masso and V. Sanz, Phys. Rev. D **87**, no. 3, 033001 (2013).
- [17] T. Corbett, O. J. P. Eboli, J. Gonzalez-Fraile and M. C. Gonzalez-Garcia, Phys. Rev. D **87**, 015022 (2013); T. Corbett, O. J. P. Eboli, J. Gonzalez-Fraile and M. C. Gonzalez-Garcia, arXiv:1306.0006 [hep-ph].
- [18] A. Falkowski, F. Riva and A. Urbano, arXiv:1303.1812 [hep-ph].
- [19] T. Plehn, D. L. Rainwater and D. Zeppenfeld, Phys. Rev. Lett. **88**, 051801 (2002).
- [20] A. Djouadi, R. M. Godbole, B. Mellado and K. Mohan, Phys. Lett. B **723**, 307 (2013).
- [21] Y. Gao, A. V. Gritsan, Z. Guo, K. Melnikov, M. Schulze and N. V. Tran, Phys. Rev. D **81**, 075022 (2010); P. Avery, D. Bourilkov, M. Chen, T. Cheng, A. Drozdetskiy, J. S. Gainer, A. Korytov and K. T. Matchev *et al.*, Phys. Rev. D **87**, 055006 (2013).
- [22] J. S. Gainer, J. Lykken, K. T. Matchev, S. Mrenna and M. Park, Phys. Rev. Lett. **111**, 041801 (2013).
- [23] J. F. Gunion, H. E. Haber and J. Wudka, Phys. Rev. D **43**, 904 (1991).
- [24] D. Choudhury, R. Islam and A. Kundu, Phys. Rev. D **88**, 013014 (2013); M. Dahiya, S. Dutta and R. Islam, arXiv:1311.4523 [hep-ph].
- [25] ATLAS conference note,
<https://atlas.web.cern.ch/Atlas/GROUPS/PHYSICS/CONFNOTES/ATLAS-CONF-2013-030/>
- [26] N. D. Christensen and C. Duhr, Comput. Phys. Commun. **180**, 1614 (2009).
- [27] J. Alwall, M. Herquet, F. Maltoni, O. Mattelaer and T. Stelzer, JHEP **1106**, 128 (2011).
- [28] T. Sjostrand, S. Mrenna and P. Z. Skands, JHEP **0605**, 026 (2006).

- [29] A. Djouadi, Phys. Rept. **457**, 1 (2008).
- [30] LHC Higgs working group,
<https://twiki.cern.ch/twiki/bin/view/LHCPhysics/CrossSections>
- [31] ATLAS conference note,
<https://atlas.web.cern.ch/Atlas/GROUPS/PHYSICS/CONFNOTES/ATLAS-CONF-2013-012/>
- [32] ATLAS conference note,
<https://atlas.web.cern.ch/Atlas/GROUPS/PHYSICS/CONFNOTES/ATLAS-CONF-2013-072/>
- [33] ATLAS conference note,
<https://atlas.web.cern.ch/Atlas/GROUPS/PHYSICS/CONFNOTES/ATLAS-CONF-2012-091/>